Adaptive Vision Token Selection for Multimodal Inference

Anonymous authors
Paper under double-blind review

Abstract

Vision encoders typically generate a large number of visual tokens, providing information-rich representations but significantly increasing computational demands. This raises the question of whether all generated tokens are equally valuable or if some of them can be discarded to reduce computational costs without compromising quality. In this paper, we introduce a new method for determining feature utility based on the idea that less valuable features can be reconstructed from more valuable ones. We implement this concept by integrating an autoencoder with a Gumbel-Softmax selection mechanism, that allows identifying and retaining only the most informative visual tokens. Experiments show that the sampler can reduce effective tokens and inference FLOPs by up to **50%** while retaining **99-100%** of the original performance on average. On challenging OCR-centric benchmarks, it also surpasses prior SOTA. The sampler transfers to the video setting as well: despite minor drops, zero-shot results remain strong without video-specific training. Our results highlight a promising direction towards adaptive and efficient multimodal pruning that facilitates scalable and low-overhead inference without compromising performance.

1 Introduction

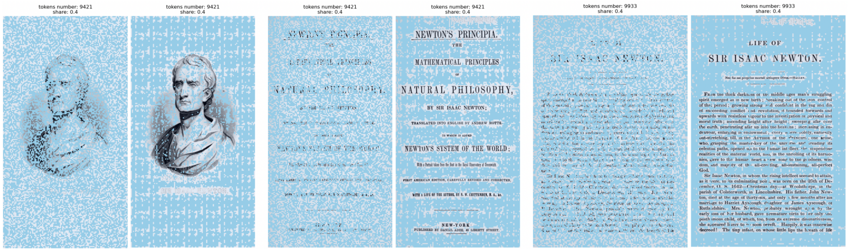

Figure 1: Comparison of feature selection methods on Newton's Principia text, in each pair of images: random feature selection retaining 40% of tokens (left), and our proposed feature selector retaining 40% of tokens (right).

In recent years, vision encoders have become important components for various downstream tasks, providing universal representation of visual features. These encoders are trained to effectively compress raw pixel information into latent embeddings. Depending on their training objectives, vision encoders can encapsulate different types of information in their hidden states. However, it is widely recognized that many of these encoded features contain redundant or irrelevant information for downstream tasks (Raghu et al., 2022; Naseer et al., 2021; Tong et al., 2024). Therefore, reducing the number of output features produced by vision encoders is an important and challenging task — especially now, as encoders increasingly serve as fundamental mechanisms for visual understanding in multimodal models (Li et al., 2024b; Chen et al., 2024c; Tong et al., 2024).

Multimodal models that process visual inputs typically condition on outputs of a Vision Transformer (ViT) (Dosovitskiy et al., 2021), appending a long vision-derived prefix to the input of a Large Language Model (LLM) via a projection layer. Although this method gives promising results, handling large context length (especially when processing high-resolution images) remains a significant challenge. Moreover, previous studies have observed that not all ViT outputs equally contribute to downstream task performance (Devoto et al., 2024); many tokens can be redundant, noisy, or simply irrelevant (Yang et al., 2024a). Therefore, selectively identifying and retaining only the most informative features can significantly decrease the number of tokens while maintaining model performance.

To address this issue, we propose a novel method to select the most informative visual features from the encoder output using an autoencoder-based approach implemented with Gumbel-Softmax sampling. Our method identifies features that are essential to preserve crucial visual information, allowing us to accurately reconstruct the original feature set. We show that this training procedure not only efficiently identifies valuable features, but also provides interpretable results, highlighting informative features that clearly correspond to specific parts of the image in the pixel space. Furthermore, we illustrate how our approach can be seamlessly integrated during inference in multimodal models, significantly reducing the visual prefix length without compromising performance.

In experiments conducted with the LLaVA-NeXT (Li et al., 2024b) with various large language models (LLMs) backbones and InternVL (Chen et al., 2024c) series of models, we demonstrate that features selected using the the proposed approach contain essential information for the model to provide the correct answer to most of the analyzed tasks. Notably, our method reduces visual context length by up to 50% with minimal performance degradation in most benchmarks. Besides, our method significantly outperforms the current SOTA approaches on the OCR-based tasks, such as document and chart question answering.

The contributions of our paper can be summarized as follows:

- We propose a novel method for selecting the most informative features from vision encoders.
- We demonstrate how our approach serves as an effective in-place feature reduction method for existing multimodal models without requiring further fine-tuning.
- We empirically confirm that retaining as little as 50% of the original visual features can be sufficient to maintain near-baseline performance on multiple multimodal benchmarks.
- Our method outperforms most existing baselines on the complex OCR-based benchmarks.

2 Related Work

Recently, several approaches for reducing context in multimodal models have been proposed, operating either at the vision-encoder level or within LLM layers and thus shortening context at different points in the stack.

2.1 Token Pruning

Pruning removes irrelevant/low–value Vision Transformer tokens while retaining salient information. Many methods use attention scores for selection (Tang et al., 2023), and some promote *diversity* to preserve broader coverage (Long et al., 2023). High-quality embeddings are especially critical for detection/segmentation (Liu et al., 2024). Task-specific variants exist; e.g., Kinfu & Vidal (2023) propose three pose-estimation pruners guided by a lightweight pose head or learnable joint tokens. The common goal is to keep tokens most informative for the downstream task.

2.2 Token Generation and Merging

A complementary line compacts representations by generating/merging tokens. TokenLearner (Ryoo et al., 2021) produces a small set of learned tokens; Token Merging (Feng & Zhang, 2023) forms “meta-tokens” by adaptively merging similar ones; (Lee & Hong, 2024) uses learnable decoupled embeddings for end-to-end merging; Resizable-ViT (Zhou & Zhu, 2023) predicts token-length labels to keep informative tokens. Hierarchical backbones such as PVT (Wang et al., 2021) downsample tokens stage-wise (static, content-agnostic), reducing cost for high-res inputs; Li et al. (2023b) further examine tokenization choices.

While effective on classic CV tasks (classification, detection, segmentation), most pruning/merging techniques are tailored to single-modal vision settings and transfer poorly to vision-language models (VLMs), which must preserve visually relevant evidence aligned with text.

2.3 Vision Context Reduction in Multimodal Models

Reducing visual context is crucial in multimodal models because visual tokens can dominate the LLM's sequence length; yet, their utility is query dependent. Existing strategies operate at different points in the stack. Interpolation–style methods downsample features while attempting to preserve salient content (e.g., LLaVA-OneVision (Li et al., 2024a)); the InternVL family (Chen et al., 2025) leverages pixel-unshuffle for high-resolution inputs; and trainable token compressors or learnable queries (e.g., Perceiver IO (Jaegle et al., 2022), BLIP-2 (Li et al., 2023c)) are built into the architecture and typically require joint training.

A more plug-and-play line prunes tokens post-hoc. FastV (Chen et al., 2024a) prunes vision tokens in selected LLM layers using attention scores from earlier layers; PyramidDrop (Xing et al., 2025) ranks image tokens with a lightweight attention module and drops a fixed fraction at multiple depths. Methods such as HiRED (Arif et al., 2024) and VisionZip (Yang et al., 2024b) select tokens using attention scores from the `[CLS]` token of the vision encoder. However, these scores degrade as pruning ratios increase (Guo et al., 2024), leading to underperformance on high-resolution, detail-dense images (e.g., text-heavy/OCR tasks). Diversity-based selectors — DivPrune (Alvar et al., 2025), PACT (Dhouib et al., 2025), and HiPrune (Liu et al., 2025) — promote coverage by clustering or maximizing token diversity and keeping the most representative tokens; some are training-free, others require light finetuning for the best performance.

The proposed method does not depend on the LLM during selection. Instead, it scores tokens by how well they preserve core visual information in the encoder's representation. Because it is training-free relative to the VLM, it can be applied directly in both purely visual (vision encoder level) and multimodal pipelines (as vision context compressor).

3 Useful Feature Selection

The Transformer architecture has been successfully used as a backbone for vision encoders (Dosovitskiy et al., 2021), providing hidden representations suitable for a wide range of vision tasks. However, due to the inherent design of the self-attention mechanism in Transformers, neighboring tokens naturally contain information about each other. Consequently, we assume that information may be duplicated redundantly in different regions of the output feature tensor. In particular, some visual representations could potentially be composed entirely of information already present in other tokens. If such redundant representations exist, they can be identified and removed without causing significant performance degradation in vision-related tasks.

This hypothesis naturally raises two critical questions: how can one quantitatively measure whether one set of features contains more information than another, and how can one select the optimal subset of features?

3.1 Feature Subset Comparison

For any image I, the corresponding feature set F has dimensions (L, C), where L is the number of vision tokens, and C is the corresponding dimension of each vision token. Tokens identified for potential exclusion have the characteristic property that they can be reconstructed from the remaining visual tokens in the set. Thus, if there exists an optimal reconstruction function R, which takes a pruned subset of features as input F^{pr} (where the superscript pr denotes *pruned*) with dimensions (L^{pr}, C) and returns a reconstructed set F^{rec} with dimensions (L, C), and if a proximity function $dist$ is defined between two tensors, then one subset is considered superior to the other if it allows for a more accurate reconstruction of the discarded visual tokens.

Formally, subset F_1^{pr} is superior to subset F_2^{pr} if:

$$dist\,(R(F_1^{pr}), F) < dist\,(R(F_2^{pr}), F)\,. \tag{1}$$

3.2 How to Select the Optimal Set?

To select the most informative features, we aim to find a function S, referred to as the *optimal selector*, which takes F as input and returns a pruned subset F^{pr}. We train this selector in a way similar to the autoencoder:

$$\min_{\theta,\psi} \operatorname{dist}\Big(R_\psi(S_\theta(F)),\, F\Big) + L^{pr}. \tag{2}$$

In this formulation, the first term provides a high-quality reconstruction of the original feature set from the pruned subset. The additional term L^{pr} penalizes the selector S_θ if it trivially selects all tokens (acting as an identity function), thereby encouraging a more concise but informative subset.

4 Method

4.1 Implementation Details

In this section, we present the implementation details of the approach described in Section 3, which consists of two main components: *Feature Selector* and *Reconstructor*.

4.1.1 Feature Selector Architecture

Feature Selector S consists of four Transformer layers and a Gumbel-Softmax-based (Jang et al., 2017) head. The head creates a binary mask, as shown in Figure 2 (left), where zeros indicate visual tokens to be removed and ones indicate tokens to be retained.

During training, feature embeddings corresponding to zeros in the binary mask are replaced by a shared learnable embedding E_{masked}, (this embedding will be reconstructed later by the component described in 4.2). During inference, embeddings corresponding to zeros are simply discarded, while those corresponding to ones are kept for downstream task. For example, they can be used as image representations in Vision-Language models, as shown in our experiments in Section 5.

For more flexibility during inference, one can choose to use logits from the linear layer instead of a hard binary mask. Based on these logits, the user can select a fixed number of the most informative features. This is exactly the approach that is used in our experiments, which we describe in Section 5.

4.2 Reconstructor Architecture

The Reconstructor is divided into two parts: a Feature Reconstructor R^f and an Image Reconstructor R^{im}.

Feature Reconstructor R^f consists of four Transformer layers and Image Reconstructor R^{im} consists of two Transformer layers and upsampling layers in interleaved with residual blocks to restore the spatial resolution. The primary objective of R^f is to restore the tokens that were replaced by the learned embedding E_{masked}, after which R^{im} should recover the image as shown in Figure 2 (left).

4.3 Loss Function

As described in Section 3.2, the optimization objective is formulated as the sum of two terms: (1) a reconstruction loss and (2) a regularization term that aims to minimize the amount of information required for reconstruction.

We decompose the reconstruction term into two parts:

$$dist(F^{rec}, F) + dist(I^{rec}, I), \tag{3}$$

where F^{rec} is reconstruction of features and I^{rec} is reconstruction of image.

In principle, we would expect the reconstruction loss to approach zero while the regularization term converges to the fraction of useful visual tokens. However, in practice we did not observe the expected behavior. We found that the optimizer is more likely to converge to a local minimum where

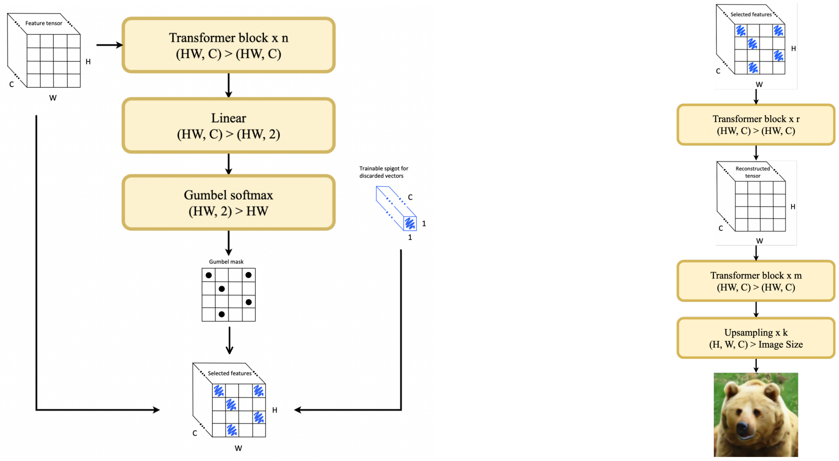

Figure 2: **Left:** Illustration of the Feature Selector in training mode. It uses four Transformer layers and a Gumbel-Softmax head to generate a binary mask where zeros mark tokens for removal and ones for retention. During training, the masked embeddings are replaced by a shared learnable embedding. During inference, the masked embeddings are discarded, while the retained ones are used for downstream tasks, such as image representations in Vision-Language models. **Right:** Illustration of Feature Reconstructor's functionality. Its primary objective is to restore the tokens that were replaced with a learned representation and then reconstruct the full image.

the regularization term drops to zero, thereby avoiding the token utilization penalty. More details can be found in Appendix B.1.

To resolve this issue, we modify the regularization term as follows.

$$L^{pr} \;\rightarrow\; \max(L^{pr},\, p) - \min(L^{pr},\, q), \tag{4}$$

where p and q specify the range of values within which the average proportion of selected tokens should fluctuate.

In other words, whenever L^{pr} falls within the interval (q, p), the regularization penalty is effectively disabled. Empirically, we observe that L^{pr} first decreases to p and then fluctuates around it for the remainder of the training period, while the reconstruction loss continues to decrease.

4.4 Training

As shown in Figure 2, our approach is similar to VQ-VAE (van den Oord et al., 2018), except that we use a set of input features instead of a learned dictionary, and the latent representation may vary in size.

We train R^f_ψ, R^{im}_ξ and S_θ following the framework introduced in 3.2. Specifically, we choose the l_2 norm for the distance function dist and compute L^{pr} using the mask generated by S_θ.

Feature Selector. The feature selector S_θ processes the original feature tensor F and outputs a subset of selected features F^{pr} along with a binary mask M, referred to as the "Gumbel mask" as illustrated in Figure 2 (right). Formally, this can be expressed as:

$$F^{pr},\, M \;=\; S_\theta(F), \tag{5}$$

where the mask M specifies which spatial locations of the input tensor F are retained (marked as ones) and which are discarded (marked as zeros). The output F^{pr}, labeled as "Selected features" in Figure 2 (left), is formed by replacing the discarded feature vectors with a shared learnable representation (shown as blue hatched vectors).

Feature Reconstructor. The reconstructor is defined by:

$$F^{rec} \;=\; R^f_\psi(F^{pr}) \;\text{ and }\; I^{rec} \;=\; R^{im}_\xi(F^{rec}), \tag{6}$$

with F^{rec} denoting the "Reconstructed tensor" shown in Figure 2 and I^{rec} denoting the image in the same figure.

Regularization Term. Regularization term is computed directly from the mask:

$$L^{pr} = \sum_{h=0,w=0}^{H,W} \frac{M_{h,w}}{HW}. \tag{7}$$

Overall Objective. Incorporating the modified regularization from 4.3, the overall optimization problem can be defined as follows:

$$\min_{\psi,\xi,\theta} \Big(\big\|F^{rec} - F\big\|_2 + \big\|I^{rec} - I\big\|_2 \Big) \; + \; \alpha_1 \cdot \, \max\big(L^{pr},\, p\big) \; - \; \alpha_2 \cdot \, \min\big(L^{pr},\, q\big) \, . \tag{8}$$

In our experiments $p = 0.6$, $q = 0.1$ and $\alpha_1 = \alpha_2 = 0.1$. All components are fully differentiable, and we optimize them using gradient descent.

4.5 Dataset

For our training dataset, we sampled 115K images from the COCO dataset (Lin et al., 2015), 9k images from DocVQA train set (Mathew et al., 2021c) and 9k images from ChartQA train set (Masry et al., 2022b). Each image was pre-processed with a specific vision encoder for which the selector was trained. The resulting feature representations were used as training data.

4.6 Training Hyperparameters

During training, we set loss weights to p=0.6, q=0.1, and α_1=α_2=0.1. Optimization uses Adam with a cosine schedule and 5% warmup. We use a batch size of 32 and train for 100 epochs in three stages (60+20+20 epochs). Learning rates are 5×10^{-6} for InternVL-like models and 1×10^{-5} for LLaVA-like models. These settings were fixed empirically and not exhaustively tuned.

5 Experiments

5.1 Experimental Setup

We evaluate our feature selector by integrating it with the vision encoders that serve as backbones in several multimodal model families: LLaVA/LLaVA-NeXT, LLaVA-Video (Zhang et al., 2025) (CLIP-based visual encoder (Radford et al., 2021)), and the InternVL (InternViT encoder (Chen et al., 2024b)) series. The method is plug-and-play: once trained for a given vision encoder, the selector can be attached to a vision — language model without any additional fine-tuning. Furthermore, a selector trained for a specific encoder can be reused across VLMs that employ that encoder, even when the encoder has been further fine-tuned during VLM training.

We test models augmented with our selector under multiple pruning ratios and compare them against the strongest recent pruning methods, including HiPrune (Liu et al., 2025), PACT (Dhouib et al., 2025), PDrop (Xing et al., 2025), FastV (Chen et al., 2024a), and DivPrune (Alvar et al., 2025). As a baseline, we also, evaluated random feature selection at matched ratios across all the tasks, to estimate whether the evaluated tasks suffer from random pruning the multimodal context.

5.2 Benchmark

We evaluate on a diverse suite of multimodal benchmarks. For general and academic-domain VQA, we use **AI2D** (Hiippala et al., 2020), **MMMU** (Yue et al., 2024), and **ScienceQA** (Lu et al., 2022). For OCR-centric tasks with high-resolution images — where preserving reading-relevant tokens is critical — we include **DocVQA** (Mathew et al., 2021b), **ChartQA** (Masry et al., 2022a), **InfoVQA** (Mathew et al., 2021a), and **TextVQA** (Singh et al., 2019). To assess hallucination sensitivity under pruned context, we additionally report results on **VizWiz** (Gurari et al., 2018) and **POPE** (Li et al., 2023d). For the video evaluation, we used 5 benchmarks ActivityNet-QA (Yu et al., 2019), SeedBench (Li et al., 2023a), NextQA (Xiao et al., 2021), EgoSchema (Mangalam et al., 2023), and LongVideoBench (Wu et al., 2024).

Table 1: Comparison of pruning approaches on Open-LLaVA-Next (Vicuna-7B). All methods are training-free. **Bold** denotes the best result with a margin of $\geq$2 percentage points (pp) over the runner-up; underline denotes results within $<$ 2 pp of the best.

Model	DocVQA	ChartQA	InfoVQA	TextVQA	SQA img	VizWiz	MMMU	Avg
2880 Tokens (100%, ≈ 21 TFLOPs)								
Original	70.5	64.1	33.1	67.3	70.4	61.8	38.1	100%
160 Tokens (5.6%, ≈ 1 TFLOP)								
HiPrune	20.8	**32.7**	20.1	40.6	67.7	54.6	36.9	64.3%
Ours	**32.0**	27.4	20.5	**54.4**	68.0	54.8	36.0	**69.4%**
320 Tokens (11.1%, ≈ 2 TFLOPs)								
DivPrune	39.7	37.9	22.1	59.6	67.4	58.7	**38.1**	76.9%
HiPrune	41.2	**42.2**	23.4	55.8	**68.2**	58.8	37.7	78.3%
Ours	**46.6**	**42.2**	24.1	**61.2**	**68.2**	57.1	35.0	**80.8%**
640 Tokens (22.2%, ≈ 4 TFLOPs)								
DivPrune	50.7	46.6	23.7	61.7	68.5	59.5	37.1	83.6%
HiPrune	58.3	47.7	26.8	60.8	69.4	60.4	38.2	87.5%
Ours	**61.9**	**57.8**	28.1	**65.7**	69.0	59.4	37.0	**92.4%**
1152 Tokens (40%, ≈ 8 TFLOPs)								
DivPrune	58.1	51.0	25.8	63.3	68.9	60.0	36.7	88.2%
HiPrune	65.6	51.6	28.7	62.3	69.4	61.1	37.3	91.7%
PDrop	64.4	58.6	32.2	65.7	69.4	61.6	38.1	95.5%
Ours	**68.3**	**63.3**	31.0	**67.2**	69.9	60.7	37.4	**97.8%**
1440 Tokens (50%, ≈ 10 TFLOPs)								
DivPrune	62.4	52.6	27.0	64.4	68.9	59.8	37.1	90.4%
HiPrune	67.2	53.0	29.0	62.4	69.2	61.2	37.3	92.6%
Ours	**69.6**	**64.2**	**32.3**	**67.2**	70.5	60.7	37.1	**99.1%**

5.3 FLOPs Calculation

Following (Chen et al., 2024a; Xing et al., 2025), we count only FLOPs attributable to *vision tokens*, including multi-head attention (MHA) and feed-forward (FFN). Let n be the number of vision tokens (e.g., 2880 for LLaVA-Next with 1+4 crops), d the hidden size (e.g., 4096), m the FFN intermediate size (e.g., 11008), and l the number of LLM layers (e.g., 32). The LLM contribution over a fraction αn tokens is

$$\mathrm{FLOPs}_{\mathrm{LLM}} = \big(4(\alpha n)d^2 + 2(\alpha n)^2 d + 2(\alpha n)dm\big)\, l.$$

Our sampler adds a *per-crop* stage over n_c tokens for each of $C = n/n_c$ crops. Using the same MHA+FFN form, with l_s sampler layers (we use $l_s = 4$),

$$\mathrm{FLOPs}_{\mathrm{sampler}} = \frac{n}{n_c}\big(4n_c d^2 + 2n_c^2 d + 2n_c dm\big)\, l_s.$$

Thus, the reported total is $\mathrm{FLOPs}_{\mathrm{total}} = \mathrm{FLOPs}_{\mathrm{LLM}} + \mathrm{FLOPs}_{\mathrm{sampler}}$.

5.4 Experimental Results

The proposed sampler-based pruning method outperforms the current SOTA overall and on OCR-centric tasks. Table 1 reports results on Open-LLaVA-Next (Vicuna-7B) (Chen & Xing, 2024). Across moderate-high pruning ratios (11-50%), our sampler consistently surpasses prior methods on **DocVQA**, **ChartQA**, and **TextVQA**; even at the most aggressive 5.6% setting, it still leads on DocVQA and TextVQA. With 50% of tokens retained, it essentially matches the unpruned model on OCR-based benchmarks.

Considering sampler overhead, the inference cost drops from ≈21 TFLOPs to ≈10 TFLOPs while retaining **99.1%** of the average performance.

Table 2: Comparison of pruning approaches on LLaVA-1.6 (Mistral-7B).

Model	DocVQA	ChartQA	InfoVQA	SQA img	MME	MMMU	AI2D	Avg
				2880 Tokens (100%)				
Original	63.6	52.9	30.5	72.6	317.5 / 1504.4	35.2	67.4	100%
				864 Tokens (30%)				
PACT	54.9	44.5	28.5	72.9	312.1 / 1484.9	34.8	67.0	95.2%
Ours	**59.8**	**50.8**	28.4	73.4	**327.1 / 1507.6**	**37.3**	66.6	**99.3%**
				1296 Tokens (45%)				
PACT	62.5	51.7	30.0	73.2	307.1 / 1504.0	34.7	67.1	99.0%
Ours	62.8	53.1	29.6	73.1	**321.8 / 1516.3**	35.6	66.9	100%

Table 2 illustrates comparison of our method with the PACT model that was applied for LLaVA-1.6 (Mistral-7B) model. At matched token budgets on LLaVA-1.6, our sampler outperforms PACT across key tasks. At 30% tokens, it improves DocVQA, ChartQA, MMMU, MME, and SQA-img and reaches **99.3%** Avg (vs. 95.2% for PACT). At 45% tokens, it again leads on most benchmarks, achieving 100% Avg (on par with the unpruned model) and even slightly exceeding the original on several tasks.

5.4.1 Video Experiments

Table 3 reports video-benchmark results with several pruning methods on LLaVA-Next-Video-7B. Although our sampler is not trained specifically for video, it transfers well, delivering strong zero-shot performance and trailing DivPrune only slightly. We anticipate further improvements with video-specific fine-tuning.

Table 3: Results on video benchmarks for LLaVA-Video-7B. All experiments use up to 8 frames per video.

Model	TFLOPs	ActivityNet	SeedBench	NextQA	EgoSch	LongVideo Bench
Original	7.8	2.49 / 49.7	43.6	27.2	40.3	43.5
FastV	1.1	1.95 / 33.9	33.0	22.5	29.1	–
DivPrune	1.1	2.45 / 48.5	41.07	26.1	40.0	42.4
Sampler (our, α =15%)	1.2	2.28 / 45.6	42.1	25.9	35.0	40.7
Sampler (our, α =10%)	0.8	2.23 / 44.7	40.8	25.5	34.3	40.1

5.5 Ablation Study

Random-token pruning. As a control, we randomly mask a fixed fraction of vision tokens at each compression rate and evaluate performance, comparing against our sampling-based selector. We further demonstrate portability beyond LLaVA by training the sampler for InternVL3 with an InternViT encoder. Figure 3 summarizes InternVL3 results across compression rates.

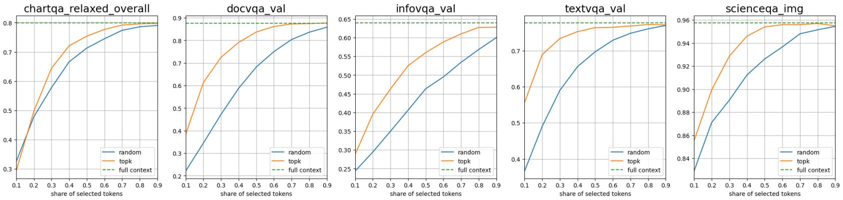

Figure 3: Comparison of InternVL3 performance across several benchmarks with various compression rate.

Across all compression rates, our sampler markedly outperforms the random baseline, indicating that these benchmarks are sensitive to vision — context pruning and that our method effectively removes irrelevant tokens from the visual input. Qualitative examples of the sampler are provided in Appendix A (Figure 6).

Sampler architecture and training epochs. We ablate the sampler on InternVL, varying encoder depth (1-8 layers) and training budget. Across the sweep, the 4-layer Transformer encoder consistently performs best, and a 100-epoch budget is required to reach the strongest results on smaller fraction of the remaining tokens. Figures 4 and 5 demonstrate INTERNVL3 performance as a function of sampler depth and training epochs, respectively.

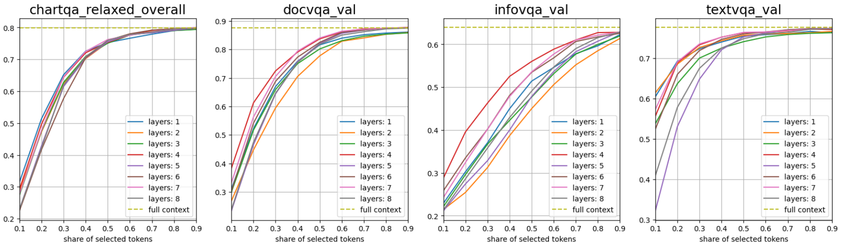

Figure 4: Sampler architecture ablation study for InternVL3 model.

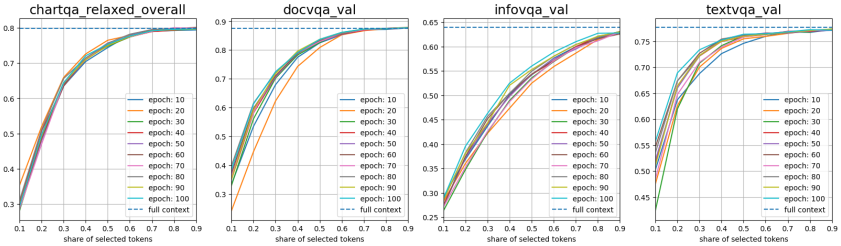

Figure 5: Training epochs ablation study for InternVL3 model.

6 CONCLUSION

We introduced a sampler-based method for selecting informative features from visual encoders. The sampler is implemented as a trainable VAE with a Gumbel–Softmax bottleneck integrated into a ViT, and it reduces the number of output vision tokens while preserving the most salient ones. We applied the method in a plug-and-play manner to modern VLMs (Open-LLaVA-Next with multiple LLM backbones and InternVL). Experiments show that the sampler can reduce effective tokens and inference FLOPs by up to **50%** while retaining **99-100%** of the original performance on average. On challenging OCR-centric benchmarks, it also surpasses prior SOTA. The sampler transfers to the video setting as well: despite minor drops, zero-shot results remain strong without video-specific training.

However, we acknowledge certain limitations of the proposed method. For long videos, compression without text conditioning can underperform. In future work, we plan joint fine-tuning of the selector and the language model, and a study of hybrid strategies that combine interpolation-style compression with Gumbel-based selection to improve compatibility and robustness.

Overall, these results point to promising directions for extracting compact, informative visual representations, enabling faster inference, lower memory footprint, and improved resilience to noisy visual inputs.

REPRODUCIBILITY STATEMENT

Section 4.4 describes the sampler's training setup, covering datasets and hyperparameters. Reproducibility code is provided in the supplementary materials. Please refer to the README file in the supplementary materials to configure the environment and reproduce the sampler training.

ETHICS STATEMENT

This work introduces a method for reducing inference compute in multimodal models and does not create new artifacts (e.g., datasets or benchmarks). All experiments use publicly available datasets and open-source models widely adopted by the community.

In this work, LLM was used exclusively for editorial refinement. It did not affect the study design, data, analysis, or outcomes.

REFERENCES

Saeed Ranjbar Alvar, Gursimran Singh, Mohammad Akbari, and Yong Zhang. Divprune: Diversity-based visual token pruning for large multimodal models, 2025. URL `https://arxiv.org/abs/2503.02175`.

Kazi Hasan Ibn Arif, JinYi Yoon, Dimitrios S. Nikolopoulos, Hans Vandierendonck, Deepu John, and Bo Ji. Hired: Attention-guided token dropping for efficient inference of high-resolution vision-language models, 2024. URL `https://arxiv.org/abs/2408.10945`.

Liang Chen, Haozhe Zhao, Tianyu Liu, Shuai Bai, Junyang Lin, Chang Zhou, and Baobao Chang. An image is worth 1/2 tokens after layer 2: Plug-and-play inference acceleration for large vision-language models, 2024a.

Lin Chen and Long Xing. Open-llava-next: An open-source implementation of llava-next series for facilitating the large multi-modal model community. `https://github.com/xiaoachen98/Open-LLaVA-NeXT`, 2024.

Zhe Chen, Jiannan Wu, Wenhai Wang, Weijie Su, Guo Chen, Sen Xing, Muyan Zhong, Qinglong Zhang, Xizhou Zhu, Lewei Lu, Bin Li, Ping Luo, Tong Lu, Yu Qiao, and Jifeng Dai. Internvl: Scaling up vision foundation models and aligning for generic visual-linguistic tasks, 2024b. URL `https://arxiv.org/abs/2312.14238`.

Zhe Chen, Jiannan Wu, Wenhai Wang, Weijie Su, Guo Chen, Sen Xing, Muyan Zhong, Qinglong Zhang, Xizhou Zhu, Lewei Lu, Bin Li, Ping Luo, Tong Lu, Yu Qiao, and Jifeng Dai. Internvl: Scaling up vision foundation models and aligning for generic visual-linguistic tasks, 2024c. URL `https://arxiv.org/abs/2312.14238`.

Zhe Chen, Weiyun Wang, Yue Cao, Yangzhou Liu, Zhangwei Gao, Erfei Cui, Jinguo Zhu, Shenglong Ye, Hao Tian, Zhaoyang Liu, Lixin Gu, Xuehui Wang, Qingyun Li, Yimin Ren, Zixuan Chen, Jiapeng Luo, Jiahao Wang, Tan Jiang, Bo Wang, Conghui He, Botian Shi, Xingcheng Zhang, Han Lv, Yi Wang, Wenqi Shao, Pei Chu, Zhongying Tu, Tong He, Zhiyong Wu, Huipeng Deng, Jiaye Ge, Kai Chen, Kaipeng Zhang, Limin Wang, Min Dou, Lewei Lu, Xizhou Zhu, Tong Lu, Dahua Lin, Yu Qiao, Jifeng Dai, and Wenhai Wang. Expanding performance boundaries of open-source multimodal models with model, data, and test-time scaling, 2025. URL `https://arxiv.org/abs/2412.05271`.

Alessio Devoto, Federico Alvetreti, Jary Pomponi, Paolo Di Lorenzo, Pasquale Minervini, and Simone Scardapane. Adaptive layer selection for efficient vision transformer fine-tuning, 2024. URL `https://arxiv.org/abs/2408.08670`.

Mohamed Dhouib, Davide Buscaldi, Sonia Vanier, and Aymen Shabou. Pact: Pruning and clustering-based token reduction for faster visual language models, 2025. URL `https://arxiv.org/abs/2504.08966`.

Alexey Dosovitskiy, Lucas Beyer, Alexander Kolesnikov, Dirk Weissenborn, Xiaohua Zhai, Thomas Unterthiner, Mostafa Dehghani, Matthias Minderer, Georg Heigold, Sylvain Gelly, Jakob Uszkoreit, and Neil Houlsby. An image is worth 16x16 words: Transformers for image recognition at scale, 2021. URL https://arxiv.org/abs/2010.11929.

Zhanzhou Feng and Shiliang Zhang. Efficient vision transformer via token merger. *IEEE Transactions on Image Processing*, 32:4156–4169, 2023. doi: 10.1109/TIP.2023.3293763.

Zhiyu Guo, Hidetaka Kamigaito, and Taro Watanabe. Attention score is not all you need for token importance indicator in kv cache reduction: Value also matters, 2024. URL https://arxiv.org/abs/2406.12335.

Danna Gurari, Qing Li, Abigale J. Stangl, Anhong Guo, Chi Lin, Kristen Grauman, Jiebo Luo, and Jeffrey P. Bigham. Vizwiz grand challenge: Answering visual questions from blind people, 2018. URL https://arxiv.org/abs/1802.08218.

Tuomo Hiippala, Malihe Alikhani, Jonas Haverinen, Timo Kalliokoski, Evanfiya Logacheva, Serafina Orekhova, Aino Tuomainen, Matthew Stone, and John A. Bateman. Ai2d-rst: a multimodal corpus of 1000 primary school science diagrams. *Language Resources and Evaluation*, 55(3):661–688, December 2020. ISSN 1574-0218. doi: 10.1007/s10579-020-09517-1. URL http://dx.doi.org/10.1007/s10579-020-09517-1.

Andrew Jaegle, Sebastian Borgeaud, Jean-Baptiste Alayrac, Carl Doersch, Catalin Ionescu, David Ding, Skanda Koppula, Daniel Zoran, Andrew Brock, Evan Shelhamer, Olivier Hénaff, Matthew M. Botvinick, Andrew Zisserman, Oriol Vinyals, and João Carreira. Perceiver io: A general architecture for structured inputs & outputs, 2022. URL https://arxiv.org/abs/2107.14795.

Eric Jang, Shixiang Gu, and Ben Poole. Categorical reparameterization with gumbel-softmax, 2017. URL https://arxiv.org/abs/1611.01144.

Kaleab Alamayehu Kinfu and René Vidal. Efficient vision transformer for human pose estimation via patch selection. In *British Machine Vision Conference*, 2023. URL https://api.semanticscholar.org/CorpusID:259096162.

Dong Hoon Lee and Seunghoon Hong. Learning to merge tokens via decoupled embedding for efficient vision transformers, 2024. URL https://arxiv.org/abs/2412.10569.

Bo Li, Yuanhan Zhang, Dong Guo, Renrui Zhang, Feng Li, Hao Zhang, Kaichen Zhang, Peiyuan Zhang, Yanwei Li, Ziwei Liu, and Chunyuan Li. Llava-onevision: Easy visual task transfer, 2024a. URL https://arxiv.org/abs/2408.03326.

Bohao Li, Rui Wang, Guangzhi Wang, Yuying Ge, Yixiao Ge, and Ying Shan. Seed-bench: Benchmarking multimodal llms with generative comprehension, 2023a. URL https://arxiv.org/abs/2307.16125.

Changzhen Li, Jie Zhang, Yang Wei, Zhilong Ji, Jinfeng Bai, and Shiguang Shan. Patch is not all you need, 2023b. URL https://arxiv.org/abs/2308.10729.

Feng Li, Renrui Zhang, Hao Zhang, Yuanhan Zhang, Bo Li, Wei Li, Zejun Ma, and Chunyuan Li. Llava-next-interleave: Tackling multi-image, video, and 3d in large multimodal models, 2024b. URL https://arxiv.org/abs/2407.07895.

Junnan Li, Dongxu Li, Silvio Savarese, and Steven Hoi. Blip-2: Bootstrapping language-image pre-training with frozen image encoders and large language models, 2023c. URL https://arxiv.org/abs/2301.12597.

Yifan Li, Yifan Du, Kun Zhou, Jinpeng Wang, Wayne Xin Zhao, and Ji-Rong Wen. Evaluating object hallucination in large vision-language models, 2023d. URL https://arxiv.org/abs/2305.10355.

Tsung-Yi Lin, Michael Maire, Serge Belongie, Lubomir Bourdev, Ross Girshick, James Hays, Pietro Perona, Deva Ramanan, C. Lawrence Zitnick, and Piotr Dollár. Microsoft coco: Common objects in context, 2015. URL https://arxiv.org/abs/1405.0312.

Jizhihui Liu, Feiyi Du, Guangdao Zhu, Niu Lian, Jun Li, and Bin Chen. Hiprune: Training-free visual token pruning via hierarchical attention in vision-language models, 2025. URL https://arxiv.org/abs/2508.00553.

Yifei Liu, Mathias Gehrig, Nico Messikommer, Marco Cannici, and Davide Scaramuzza. Revisiting token pruning for object detection and instance segmentation. In *Proceedings of the IEEE/CVF Winter Conference on Applications of Computer Vision (WACV)*, 2024.

Sifan Long, Zhen Zhao, Jimin Pi, Shengsheng Wang, and Jingdong Wang. Beyond Attentive Tokens: Incorporating Token Importance and Diversity for Efficient Vision Transformers . In *2023 IEEE/CVF Conference on Computer Vision and Pattern Recognition (CVPR)*, pp. 10334–10343, Los Alamitos, CA, USA, June 2023. IEEE Computer Society. doi: 10.1109/CVPR52729.2023.00996. URL https://doi.ieeecomputersociety.org/10.1109/CVPR52729.2023.00996.

Pan Lu, Swaroop Mishra, Tony Xia, Liang Qiu, Kai-Wei Chang, Song-Chun Zhu, Oyvind Tafjord, Peter Clark, and Ashwin Kalyan. Learn to explain: Multimodal reasoning via thought chains for science question answering, 2022. URL https://arxiv.org/abs/2209.09513.

Karttikeya Mangalam, Raiymbek Akshulakov, and Jitendra Malik. Egoschema: A diagnostic benchmark for very long-form video language understanding, 2023. URL https://arxiv.org/abs/2308.09126.

Ahmed Masry, Do Xuan Long, Jia Qing Tan, Shafiq Joty, and Enamul Hoque. Chartqa: A benchmark for question answering about charts with visual and logical reasoning, 2022a. URL https://arxiv.org/abs/2203.10244.

Ahmed Masry, Do Xuan Long, Jia Qing Tan, Shafiq Joty, and Enamul Hoque. Chartqa: A benchmark for question answering about charts with visual and logical reasoning, 2022b. URL https://arxiv.org/abs/2203.10244.

Minesh Mathew, Viraj Bagal, Rubèn Pérez Tito, Dimosthenis Karatzas, Ernest Valveny, and C. V Jawahar. Infographicvqa, 2021a. URL https://arxiv.org/abs/2104.12756.

Minesh Mathew, Dimosthenis Karatzas, and C. V. Jawahar. Docvqa: A dataset for vqa on document images, 2021b. URL https://arxiv.org/abs/2007.00398.

Minesh Mathew, Dimosthenis Karatzas, and C. V. Jawahar. Docvqa: A dataset for vqa on document images, 2021c. URL https://arxiv.org/abs/2007.00398.

Muzammal Naseer, Kanchana Ranasinghe, Salman Khan, Munawar Hayat, Fahad Shahbaz Khan, and Ming-Hsuan Yang. Intriguing properties of vision transformers, 2021. URL https://arxiv.org/abs/2105.10497.

Alec Radford, Jong Wook Kim, Chris Hallacy, Aditya Ramesh, Gabriel Goh, Sandhini Agarwal, Girish Sastry, Amanda Askell, Pamela Mishkin, Jack Clark, Gretchen Krueger, and Ilya Sutskever. Learning transferable visual models from natural language supervision, 2021. URL https://arxiv.org/abs/2103.00020.

Maithra Raghu, Thomas Unterthiner, Simon Kornblith, Chiyuan Zhang, and Alexey Dosovitskiy. Do vision transformers see like convolutional neural networks?, 2022. URL https://arxiv.org/abs/2108.08810.

Michael Ryoo, AJ Piergiovanni, Anurag Arnab, Mostafa Dehghani, and Anelia Angelova. Tokenlearner: Adaptive space-time tokenization for videos. In M. Ranzato, A. Beygelzimer, Y. Dauphin, P.S. Liang, and J. Wortman Vaughan (eds.), *Advances in Neural Information Processing Systems*, volume 34, pp. 12786–12797. Curran Associates, Inc., 2021. URL https://proceedings.neurips.cc/paper_files/paper/2021/file/6a30e32e56fce5cf381895dfe6ca7b6f-Paper.pdf.

Amanpreet Singh, Vivek Natarajan, Meet Shah, Yu Jiang, Xinlei Chen, Dhruv Batra, Devi Parikh, and Marcus Rohrbach. Towards vqa models that can read, 2019. URL https://arxiv.org/abs/1904.08920.

Quan Tang, Bowen Zhang, Jiajun Liu, Fagui Liu, and Yifan Liu. Dynamic token pruning in plain vision transformers for semantic segmentation. In *2023 IEEE/CVF International Conference on Computer Vision (ICCV)*, pp. 777–786, 2023. doi: 10.1109/ICCV51070.2023.00078.

Shengbang Tong, Ellis Brown, Penghao Wu, Sanghyun Woo, Manoj Middepogu, Sai Charitha Akula, Jihan Yang, Shusheng Yang, Adithya Iyer, Xichen Pan, Ziteng Wang, Rob Fergus, Yann LeCun, and Saining Xie. Cambrian-1: A fully open, vision-centric exploration of multimodal llms, 2024. URL https://arxiv.org/abs/2406.16860.

Aaron van den Oord, Oriol Vinyals, and Koray Kavukcuoglu. Neural discrete representation learning, 2018. URL https://arxiv.org/abs/1711.00937.

Wenhai Wang, Enze Xie, Xiang Li, Deng-Ping Fan, Kaitao Song, Ding Liang, Tong Lu, Ping Luo, and Ling Shao. Pyramid vision transformer: A versatile backbone for dense prediction without convolutions. In *2021 IEEE/CVF International Conference on Computer Vision (ICCV)*, pp. 548–558, 2021. doi: 10.1109/ICCV48922.2021.00061.

Haoning Wu, Dongxu Li, Bei Chen, and Junnan Li. Longvideobench: A benchmark for long-context interleaved video-language understanding, 2024. URL https://arxiv.org/abs/2407.15754.

Junbin Xiao, Xindi Shang, Angela Yao, and Tat-Seng Chua. Next-qa: Next phase of question-answering to explaining temporal actions. In *Proceedings of the IEEE/CVF Conference on Computer Vision and Pattern Recognition (CVPR)*, pp. 9777–9786, June 2021.

Long Xing, Qidong Huang, Xiaoyi Dong, Jiajie Lu, Pan Zhang, Yuhang Zang, Yuhang Cao, Conghui He, Jiaqi Wang, Feng Wu, and Dahua Lin. Pyramiddrop: Accelerating your large vision-language models via pyramid visual redundancy reduction, 2025. URL https://arxiv.org/abs/2410.17247.

Jiawei Yang, Katie Z Luo, Jiefeng Li, Congyue Deng, Leonidas Guibas, Dilip Krishnan, Kilian Q Weinberger, Yonglong Tian, and Yue Wang. Denoising vision transformers, 2024a. URL https://arxiv.org/abs/2401.02957.

Senqiao Yang, Yukang Chen, Zhuotao Tian, Chengyao Wang, Jingyao Li, Bei Yu, and Jiaya Jia. Visionzip: Longer is better but not necessary in vision language models, 2024b. URL https://arxiv.org/abs/2412.04467.

Zhou Yu, Dejing Xu, Jun Yu, Ting Yu, Zhou Zhao, Yueting Zhuang, and Dacheng Tao. Activitynet-qa: A dataset for understanding complex web videos via question answering, 2019. URL https://arxiv.org/abs/1906.02467.

Xiang Yue, Yuansheng Ni, Kai Zhang, Tianyu Zheng, Ruoqi Liu, Ge Zhang, Samuel Stevens, Dongfu Jiang, Weiming Ren, Yuxuan Sun, Cong Wei, Botao Yu, Ruibin Yuan, Renliang Sun, Ming Yin, Boyuan Zheng, Zhenzhu Yang, Yibo Liu, Wenhao Huang, Huan Sun, Yu Su, and Wenhu Chen. Mmmu: A massive multi-discipline multimodal understanding and reasoning benchmark for expert agi, 2024. URL https://arxiv.org/abs/2311.16502.

Yuanhan Zhang, Jinming Wu, Wei Li, Bo Li, Zejun Ma, Ziwei Liu, and Chunyuan Li. Llava-video: Video instruction tuning with synthetic data, 2025. URL https://arxiv.org/abs/2410.02713.

Qiqi Zhou and Yichen Zhu. Make a long image short: Adaptive token length for vision transformers. In Danai Koutra, Claudia Plant, Manuel Gomez Rodriguez, Elena Baralis, and Francesco Bonchi (eds.), *Machine Learning and Knowledge Discovery in Databases: Research Track*, pp. 69–85, Cham, 2023. Springer Nature Switzerland. ISBN 978-3-031-43415-0.

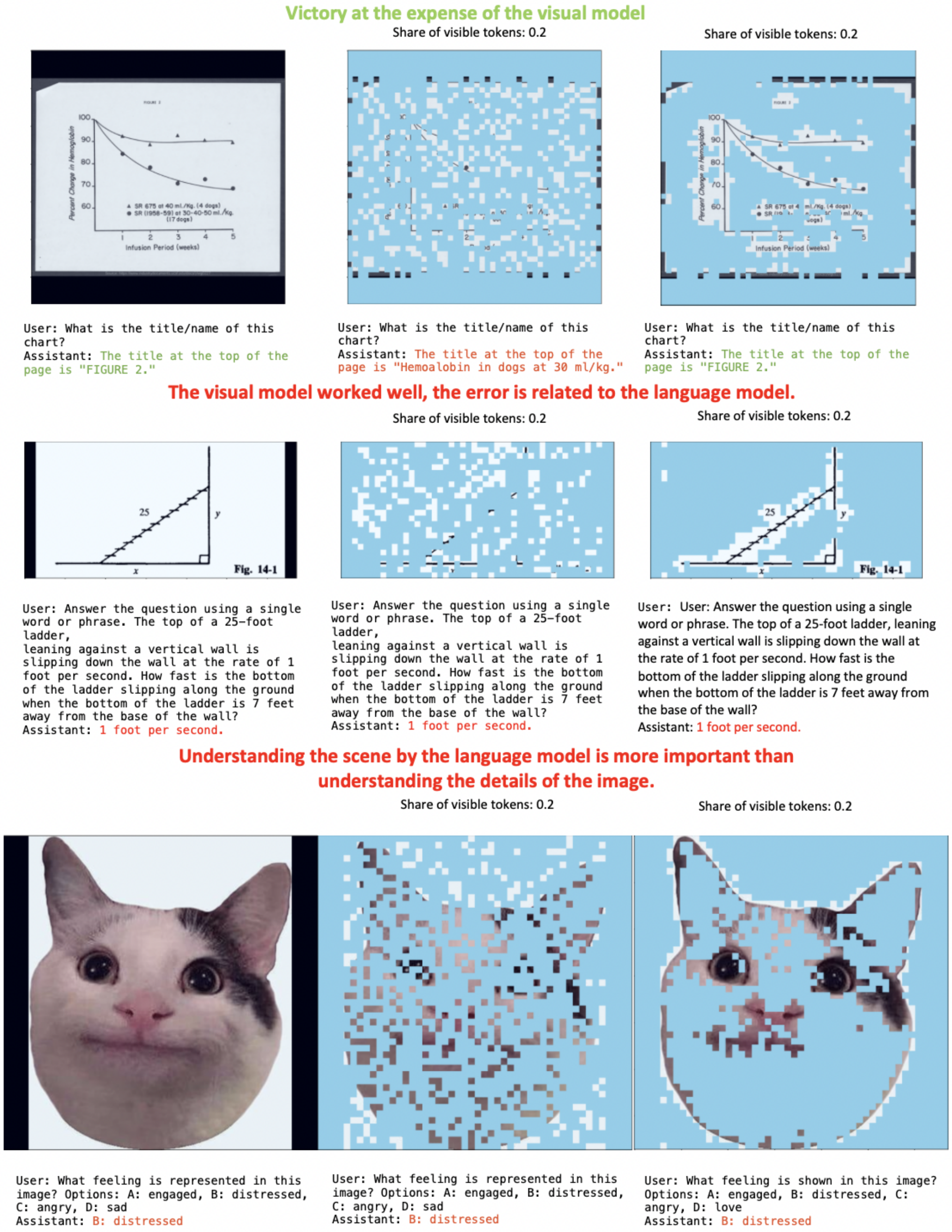

Victory at the expense of the visual model

Share of visible tokens: 0.2

Share of visible tokens: 0.2

User: What is the title/name of this chart?
Assistant: The title at the top of the page is "FIGURE 2."

User: What is the title/name of this chart?
Assistant: The title at the top of the page is "Hemoalobin in dogs at 30 ml/kg."

User: What is the title/name of this chart?
Assistant: The title at the top of the page is "FIGURE 2."

The visual model worked well, the error is related to the language model.

Share of visible tokens: 0.2

Share of visible tokens: 0.2

User: Answer the question using a single word or phrase. The top of a 25-foot ladder,
leaning against a vertical wall is slipping down the wall at the rate of 1 foot per second. How fast is the bottom of the ladder slipping along the ground when the bottom of the ladder is 7 feet away from the base of the wall?
Assistant: 1 foot per second.

User: Answer the question using a single word or phrase. The top of a 25-foot ladder,
leaning against a vertical wall is slipping down the wall at the rate of 1 foot per second. How fast is the bottom of the ladder slipping along the ground when the bottom of the ladder is 7 feet away from the base of the wall?
Assistant: 1 foot per second.

User: User: Answer the question using a single word or phrase. The top of a 25-foot ladder, leaning against a vertical wall is slipping down the wall at the rate of 1 foot per second. How fast is the bottom of the ladder slipping along the ground when the bottom of the ladder is 7 feet away from the base of the wall?
Assistant: 1 foot per second.

Understanding the scene by the language model is more important than understanding the details of the image.

Share of visible tokens: 0.2

Share of visible tokens: 0.2

User: What feeling is represented in this image? Options: A: engaged, B: distressed, C: angry, D: sad
Assistant: B: distressed

User: What feeling is represented in this image? Options: A: engaged, B: distressed, C: angry, D: sad
Assistant: B: distressed

User: What feeling is shown in this image? Options: A: engaged, B: distressed, C: angry, D: love
Assistant: B: distressed

Figure 6: Images from three benchmarks illustrating cases where the vision-language model gives correct answers or makes errors. The first column shows the model's responses using the full visual context, the second column uses a randomly selected set of features, and the third column uses the features selected by our selector. (1) DocVQA: to answer the question selecting the correct features is crucial. (2) MMMU (math): to answer this question, both visual understanding and logical reasoning are important, but the model fails to reason correctly. (3) MMstar: the image details are less important, and the language model plays a dominant role.

A Qualitative Examples

A.1 Selector on various feature percentage

Figure 6 illustrates the effect of keeping only 20% of vision tokens. From left to right: original image, tokens kept by random selection, and tokens kept by our sampler. Compared to random, the sampler focuses on regions that contain the most informative content, which in turn improves the model's answer to the final question.

A.2 Failed examples

In this section, we evaluate failure cases in which the VLM's answers degrade when the feature selector is applied. To investigate the causes of such failures, we analyzed detailed logs of the model's predictions on the benchmarks, focusing specifically on cases where the initial model answer was correct but, after applying the selector, the model changed its answer to an incorrect one. Based on the observed performance degradation at specific feature levels, we propose the following hypotheses:

- The selector did not retain specific image features that are crucial for answering the question.
- The model itself could not adapt to the modified distribution of image features and failed to answer correctly even when the mask contained the necessary information.

Our analysis shows that most failures correspond to the second hypothesis. In other words, in most cases all the information necessary to answer the question was present in the image, however, the model could not successfully leverage it and changed its answer. Please refer to Figure 7 for more details.

We hypothesize that this behavior is caused by the specifics of the model's training: changing the standard number of vision tokens to a sparser set may lead to performance degradation. In future work, we will study this effect in more detail by performing ablations and fine-tuning the model on the reduced feature space, then comparing performance.

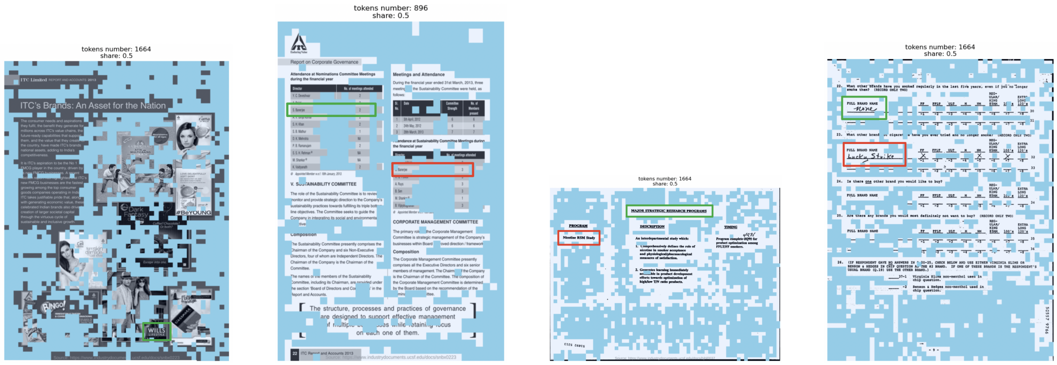

(a) **Question:** What is the name of the fashion wear/clothing advertise?
Target: Wills Lifestyle
Answer: WILLS

(b) **Question:** How many nomination committee meetings has S. Banerjee attended?
Target: 2
Answer: 3

(c) **Question**: What is the name of the research program?
Target: MAJOR STRATEGIC RESEARCH PROGRAMS
Answer: nicotine rsm study

(d) **Question**: What is the brand name for the 22nd question?
Target: none
Answer: lucky strike

Figure 7: Examples of model errors. Green boxes indicate areas containing the correct answer, red boxes indicate areas that the model likely focused on when providing the answer.

We observe that the information necessary to provide the correct answer remains visible after applying the mask; however, the model is no longer able to answer correctly, even though its answer on the full image was correct.

B Ablation Study

B.1 Gumbel usage ablation

Equation 8 presents the loss function used to optimize the network. In Section 4.3, we explained that the term $\alpha_1 \cdot L^{pr}$ is replaced by the term $\alpha_1 \cdot \ max\big(L^{pr},\, p\big) - \alpha_2 \cdot \ \min\big(L^{pr},\, q\big)$. Otherwise, we observed that the optimizer falls into a local minimum of the term L^{pr}, i.e., it drives $L^{pr} = 0$.

It turns out that this behavior of the optimizer is related to the use of Gumbel Softmax for computing the Gumbel mask (the mask of sampled tokens). When using a simple straight-through estimator ($y_{hard} - y_{soft}.detach() + y_{soft}$, where y_{soft} is the Softmax), the problem of getting stuck in a local minimum is not observed, meaning the standard term $\alpha_1 \cdot L^{pr}$ can be used in the loss function.

We compared three versions for selector training objectives:

- (Our) Gumbel Softmax + $\Big(\big\|F^{rec} - F\big\|_2 + \big\|I^{rec} - I\big\|_2\Big) \ + \ \alpha_1 \cdot \ \max\big(L^{pr},\, p\big) \ - \ \alpha_2 \cdot \min\big(L^{pr},\, q\big)$.
- Simple straight-through estimator + $\Big(\big\|F^{rec} - F\big\|_2 + \big\|I^{rec} - I\big\|_2\Big) \ + \ \alpha_1 \cdot \ L^{pr}$.
- Simple straight-through estimator + $\Big(\big\|F^{rec} - F\big\|_2 + \big\|I^{rec} - I\big\|_2\Big) \ + \alpha_1 \cdot \max\big(L^{pr},\, p\big) \ - \alpha_2 \cdot \ \min\big(L^{pr},\, q\big)$.

Figure 8 shows the benchmark performance of the InternVL3 model on four representative benchmarks, with the selectors fine-tuned using different methods. Apart from the differences described above, the training pipelines are identical in all experiments $\alpha_1 = \alpha_2 = 0.1$. We observe that higher performance at lower token percentages is obtained by training with Gumbel addition, thus, the randomness introduced by Gumbel addition acts as a form of regularization.

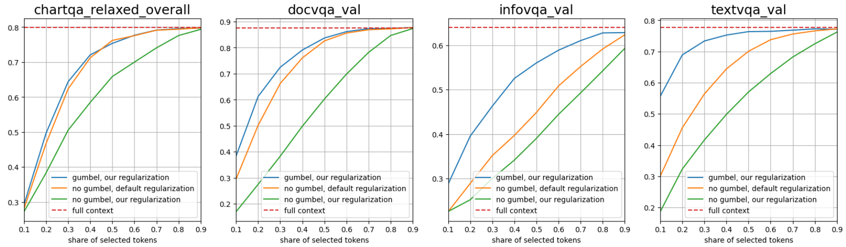

Figure 8: A comparison of training objective: (*blue*) Gumbel Softmax with the proposed loss regularization; (*orange*) straight-through estimator with the standard L_{pr} term; (*green*) straight-through estimator with the proposed loss regularization.

B.2 Instability of "Gumbel Softmax + loss with a standard regularization term" approach

In some of our experiments, we attempted to train a feature selector using a Gumbel Softmax + loss with a standard regularization term: $\Big(\big\|F^{rec} - F\big\|_2 + \big\|I^{rec} - I\big\|_2\Big) \ + \ \alpha_1 \cdot \ L^{pr}$. However, this method proved to be very sensitive to training hyperparameters. An example of training graphs in such a pipeline is shown in Figure 9. We believe that there exists an optimal subset of hyperparameters for which such training would be stable; however, searching for it is quite resource-consuming, so we instead chose to improve the regularization term so that regularization is disabled in the case of collapse described in Equation 4.

B.3 The stability of our approach

As shown in Figure 9 in the previous section, using a regularization term of the form $\alpha_1 \cdot \ L^{pr}$ leads to training instability, manifested by the regularization term collapsing to zero. Figure 10 shows the

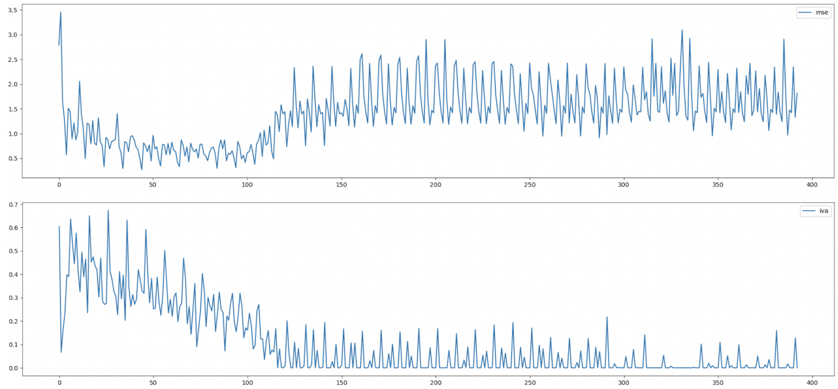

Figure 9: Selector training curves for the InternVL model with the Gumbel Softmax pipeline + loss with standard regularization. The curve on top corresponds to term $\|F^{rec} - F\|_2 + \|I^{rec} - I\|_2$. The curve on the bottom corresponds to term $\alpha_1 \cdot \ L^{pr}$.

optimization results with our regularization term $\alpha_1 \cdot \ \max\big(L^{pr},\, p\big) \ - \ \alpha_2 \cdot \ \min\big(L^{pr},\, q\big)$. As can be seen, the nature of the dynamics changes dramatically: from a certain point, the regularization term begins to fluctuate around the value p. This prevents training degradation and ensures a more robust reconstruction loss optimization process.

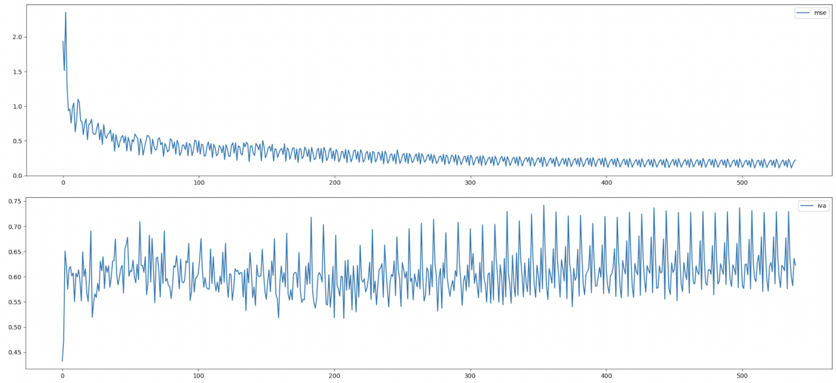

Figure 10: Selector training curves for the InternVL model with the Gumbel Softmax pipeline + loss with our regularization term. The graph on top corresponds to term $\|F^{rec} - F\|_2 + \|I^{rec} - I\|_2$. The curve on the bottom corresponds to our regularization term $\alpha_1 \cdot \ \max\big(L^{pr},\, p\big) \ - \ \alpha_2 \cdot \ \min\big(L^{pr},\, q\big)$.

B.4 Conditional Selection

The proposed approach operates at the vision-encoder level, allowing us to reduce the number of vision tokens while preserving the most essential information about the image. One promising direction for future work is to condition the feature selector on the text query. To achieve this, we change the learning and insight extraction strategy. Specifically, instead of feeding the selector with features from the visual encoder, we provide it with features from a certain LLM layer, which are already enriched with textual information. Examples of such conditioned sampling are shown in Figure 11.

We found that our approach works when placing the question before the image. However, reversing the image and question significantly impacts the baseline model's metrics. We also found that the metrics drop less when placing the question both before and after the image.

Table 4: Comparison of the original InternVL3-2B model and the same model with a conditional selection of features.

Model	DocVQA	ChartQA	InfoVQA	TextVQA	MME	GQA	POPE	SQA img	VizWiz
Original	82.3	71.8	52.8	73.7	413.2 / 1320.2	54.0	89.5	81.6	60.7
w/ Condition (middle layer)	83.1	72.4	53.1	73.9	427.9 / 1300.7	54.7	89.0	81.8	60.8

The Table 4 shows the results of a comparison between the original model and the same one with middle-layer conditioning (that is, only question-relevant tokens remain after the middle layer). In both cases, the question is presented as $\langle question \rangle + \langle image \rangle + \langle question \rangle$.

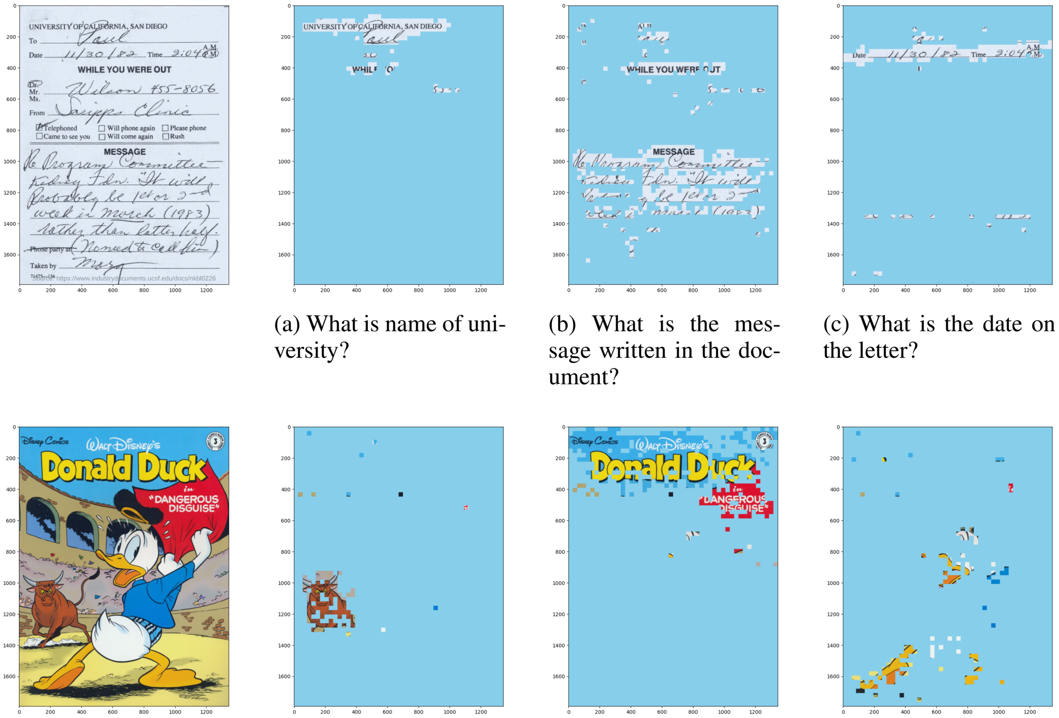

(a) What is name of university?

(b) What is the message written in the document?

(c) What is the date on the letter?

(d) What color is a bull's skin?

(e) What text on the image is?

(f) What color is the skin on a duck's legs?

Figure 11: Examples of conditional selectors in action. Each example is accompanied by the question for which the mask was generated.

B.5 Stability of the selection mask

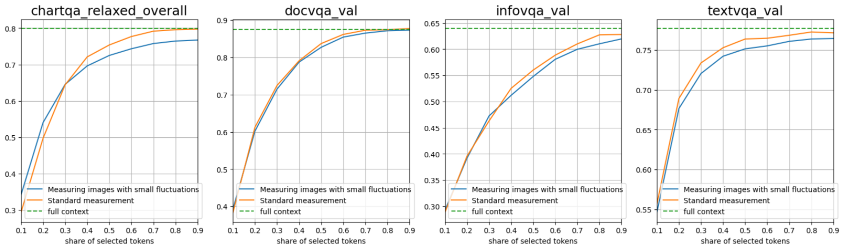

Figure 12: Stability of the selection mask ablation study for InternVL3 model.

To test the mask's robustness to small distortions, we applied two transformations to the images. First, we cropped up to five percent of the image on each side independently (the crop percentage was randomly selected). Second, we varied the brightness with a random coefficient in the range of 0.8-1.2. The measurement results are shown in the Figure 12.